ROYAL OBSERVATORY, HONG KONG

Technical Note (Local) No. 53

THE ROYAL OBSERVATORY NUMERICAL ANALYSIS-FORECASTING SYSTEM

by

CHAN Yuk-kwan

Published December 1989

Prepared by

Royal Observatory
134A Nathan Road
Kowloon
Hong Kong

551.509.313(512.317)

CONTENTS

FIGURES

TABLES

1. INTRODUCTION

There has been an increasing demand from the public and the private sectors for more precise weather forecasts in terms of timing, location, spatial distribution and intensity of weather phenomena.

For some years, the Royal Observatory (RO) has been using outputs from numerical weather prediction models of the European Centre for Medium Range Weather Forecasts (ECMWF) and the United Kingdom Meteorological Office (UKMO) as guidance in the preparation of its HK forecasts. These products have proved valuable in the daily operation of the provision of weather services to the public and in the research work of the development of forecasting aids. However, this information is transmitted over the Global Telecommunication System at reduced resolution. Thus, it is adequate only for predicting large-scale weather systems such as surges of the winter monsoon, but inadequate for meso-scale features such as monsoon troughs which are often the cause of inclement weather conditions.

There is a need to develop, for application in Hong Kong, a fine resolution analysis-forecasting system which will provide an objective means of assimilating all the available data and predicting the evolution of the meso-scale features. With such a view in mind, an attempt was carried out in the RO to adapt the two dimensional multivariate optimal interpolation data analysis scheme (OI) and the very fine mesh limited area model (VFM65) of the Japan Meteorological Agency (JMA) for application in the domain around Hong Kong. Due to the limited capacity of the RO's computer system, a numerical weather prediction model in a domain larger than the present one cannot be run to provide the lateral boundary condition operationally. Thus, arrangement was made with JMA to transmit boundary data from their Global Spectral Model to Hong Kong everyday for use in the daily operational runs of our models.

This technical note provides an account of the mathematical, physical and computational aspects of the adapted numerical models. It also describes briefly the performance of the models over a one-month period when the analysis-forecasting system was first put into operation on a trial basis. In-depth and systematic subjective and objective verification of the model outputs, however, is the subject matter of a separate report. The details in the coding and the operation of the analysis-forecasting system are given in the operation manual by Chan (1988).

2. THE OPTIMAL INTERPOLATION DATA ANALYSIS SCHEME

The analysis scheme is a two dimensional multivariate optimal interpolation scheme performed on 10 standard pressure levels in the vertical. The vertical structure of the analysed field is shown in Figure 1. The horizontal domain of the analyses is shown in Figure 2. The domain is covered by a 101 x 66 latitude-longitude grid of one degree resolution. The grid length is 111.2 km true at 22.5 N.

(a) Formulation of the analysis scheme

The analysis scheme is based on the optimal interpolation method (Schlatter, 1975) which is outlined as follows.

Let X denote any meteorological variable, n the number of variables used in the analysis, w the weights to be determined and σ^p the standard deviation of the prediction error. Then, the interpolated value at a grid point from irregularly spaced observations is estimated by

$$X_g^I = X_g^p + \sum_{i=1}^{n} w_i \, (X_i^o - X_i^p) \, \sigma_g^p / \sigma_i^p \qquad (2.1)$$

where superscripts 'o', 'p' and 'I' indicate observed, predicted and interpolated values respectively; subscript 'g' represents grid-point values of the variable to be analysed and subscript 'i' the observation values of the variables used in the analysis. In JMA, the predicted values from the Asian Model serve as the first guess field. In the Hong Kong context, such values are not available and an extended area model is being tested to provide predicted values as the first guess field. For the time being, the first guess field is a coarse resolution analysis using the Cressman scheme.

In general, X_g^I in equation (2.1) will differ from the true value at the grid point by an amount known as the analysis error. The weights are determined such that the mean square analysis error $(E_g^I)^2$ over a large number of analysis situations is minimized. As the observations are usually made without any knowledge of the predicted values, the prediction errors and observation errors are assumed to be uncorrelated. The minimization is equivalent to the requirement that $\partial (E_g^I)^2 / \partial w_i = 0$ which leads to a set of normal equations :

$$\sum_{j=1}^{n} (\mu_{ij}^p + \mu_{ij}^o \, \lambda_i \lambda_j) \, w_j = \mu_{ig}^p \qquad (i=1,2,....n) \qquad (2.2)$$

$$\lambda_i = \sigma_i^o / \sigma_i^p$$

u^p and u^o denote prediction and observation error correlation coefficients respectively, and σ^o is the standard deviation of the observation error.

In general, X_i and X_g in equation (2.1) can be different with respect to the type of variable, vertical level and time. To meet operational time limits, a two-dimensional form is used in our analysis scheme. That is, only variables in the same vertical level are used.

The method of analysis of a meteorological element depends upon the latitude. Over the extratropical region north of 25 degrees north, multivariate method is used for the analysis of height and wind at all levels except at the surface. However, over the subtropical region between 15 and 25 degrees north, the wind-height correlations are multiplied by an empirical coefficient which depends on latitude in order to gradually decouple the wind and height analyses. Over the tropics south of 15 degrees north, where the geostrophic relation is inappropriate, winds are analysed using a bivariate method, and the geopotential heights by a univariate method.

Temperature and dew point depression are analysed by univariate method.

(b) Determination of statistical parameters

Assuming homogeneity and isotropy, the prediction error auto-correlation for height, temperature and dew point depression are given by

$$\mu^p_{ij} = \exp(-br^2_{ij}) \qquad (2.3)$$

where b is a constant which depends on the variable used in the analysis, the level of the analysis and the latitude of the variables to tbe analysed; and r_{ij} the distance between points i and j. In JMA, the prediction error correlations (correlations of the difference between prediction and observation) for different pairs of observation points were computed over East Asia, United States of America, Europe and USSR. Then, using these correlations, the values of b were estimated by the same procedure in Alaka and Elvander (1972).

The wind-wind and wind-height prediction error correlations over the extratropical region are derived from the height-height correlation using the geostrophic relation. From equation (2.3) for the height-height correlation, the following relations are obtained.

$$\mu^p(z_i u_j) = -\sqrt{2}b\ (y_i - y_j)\ \mu^p(z_i z_j) \tag{2.4a}$$

$$\mu^p(z_i v_j) = -\sqrt{2}b\ (x_i - x_j)\ \mu^p(z_i z_j) \tag{2.4b}$$

$$\mu^p(u_i u_j) = \{1 - 2b\ (y_i - y_j)^2\}\ \mu^p\ (z_i z_j) \tag{2.4c}$$

$$\mu^p(v_i v_j) = \{1 - 2b\ (x_i - x_j)^2\}\ \mu^p\ (z_i z_j) \tag{2.4d}$$

$$\mu^p(u_i v_j) = 2b\ (x_i - x_j)(y_i - y_j)\mu^p(z_i z_j) \tag{2.4e}$$

$\mu^p(X_i Y_j)$ denotes the prediction error correlation between variable X at point i and variable Y at point j.

In the tropics, the wind-wind correlations are derived from the stream function correlation under the assumption of non-divergent flow. These correlation coefficients have the same form as those in equatons (2.4) except that $\mu^p(z_i z_j)$ is replaced by $\mu^p(\psi_i \psi_j)$ where ψ is the streamfunction. The values of b for $\mu^p(\psi_i \psi_j)$ are assumed to be the same as for $\mu^p(z_i z_j)$.

The observation error correlation of SATEMs is also modelled by equation (2.3), but with $b = 11.3 \times 10^{-6}$ km^{-2} (Bergman, 1979). No observation error correlation is assumed for other types of data.

The standard deviation of observation error for radiosonde data was modelled in a fashion similar to Kurihara (1961) and Lenhard (1970), but also considering the following statistics :

(i) root-mean-square differences between observation and analysed values over the data rich regions;

(ii) root-mean-square and correlation of the apparent prediction error.

The standard deviations of observation error for other types of data and the standard deviation of prediction error are modelled using the root-mean-square differences between other observations or predictions and the collocated radiosonde data.

As the JMA statistical coefficients were determined to 'optimize' the analyses in the domain around Japan, they may not 'optimize' the analyses around Hong Kong simultaneously. Thus, statistical coefficients have to be re-derived for the RO model domain. At present, the statistical coefficients for pressure/height and temperature have already been replaced (Figure 3). Effort is now concentrated on re-deriving the coefficients for humidity.

(c) Data selection procedure

Here we do not have trials of our own to determine the optimal 'sphere of influence'. The data selection procedure of JMA is adopted. The maximum number of data to be used at one grid point was decided from some trial analyses using real data, and model experiments using idealized observation networks. Boxes with sides of 5, 10, 15, 20, 25 and 30 degrees of latitude, centred on the grid point, are scanned until the M closest variable are selected or the largest box is scanned. The scanning for each grid point is started from the box size pre-determined by the statistics of data distribution. M is set to 10 in the univariate case and varies from 30 at lower levels to 45 at upper levels in the multivariate case. All the variables at one observation point are simultaneously used in the multivariate case. If there is only one or no observation point in the largest box, the first guess value is used.

(d) Generation of bogus data for tropical cyclones

Genesis and development of tropical cyclones usually take place over oceans where few observations are available. It is therefore necessary to inject bogus data into the objective analysis to improve the representation of tropical cyclones.

The numerical scheme to generate bogus data for tropical cyclone in the JMA VFM65 (Ueno, 1989) covers : the low- and mid-level circulations, the warm core and the upper-level divergence field. The initial internal balance among the data is achieved by applying the limited area normal mode initialization scheme.

As no initialization scheme, except smoothing, is used in the Royal Observatory numerical analysis-forecasting system, only the following bogus data are generated empirically based on a Rankine type model (Anderson and Hollingsworth, 1988) :

(i) mean-sea-level pressure,
(ii) winds at 850, 700 and 500 hPa.

The generated fields are spherically symmetric and computed from the following manually analysed data :

(i) central position,
(ii) central pressure,
(iii) radius and pressure at radius of strong wind,
(iv) radius and value of outermost closed isobar.

The internal balance among the bogus data is achieved during forward integration in time.

3. THE ROYAL OBSERVATORY LIMITED AREA MODEL

The RO limited area model is adapted from the JMA VFM65 (JMA, 1986). It is a three dimensional primitive equation model in sigma coordinate. In the design of the model, emphasis is placed in the simulation of small scale features of the atmosphere, especially those caused by the surface conditions of the earth such as orography and land-sea contrast. Thus, the model has a high vertical resolution in the lower troposphere (see Figure 4) and a fairly sophiscated scheme for the parameterization of the boundary layer.

(a) Model structure

The model uses sigma coordinate and has 13 layers in the vertical. The arrangement of the sigma levels is shown in Table 1. Sigma is defined as follows :

$$\sigma = (p - p_t) / \pi$$

$$\pi = p_s - p_t$$

$$p_s = p_s(x, y, t)$$

p is the pressure, p_t (= 100 hPa) the pressure at the top of the model atmosphere and p_s the surface pressure.

It is easy to show that when $p = p_s$ or p_t, the corresponding sigma values are 1 and 0 respectively. It is also obvious that the top and the bottom boundary conditions of the model can be expressed as

$$\dot{\sigma} = 0 \quad \text{when} \quad \sigma = 1 \text{ or } 0$$

All the variables (i.e. u, v the two horizontal components of the wind velocity, θ the potential temperature, q the specific humidity and ϕ the geopotential) are defined on the specified sigma levels with the exception of $\dot{\sigma}$, vertical fluxes and eddy diffusivities for momentum, heat and water vapor, which are defined at the intermediate levels.

Figure 5 shows the horizontal domain of the model. The domain is covered by a 51 x 36 one degree grid in latitude-longitude projection. The grid-length is 111.2 km true at 22.5 N. In the horizontal, all the variables are defined at the same grid point. Thus, the grid is a non-staggered one (Arakawa A-grid). Apparently, no decoupling or other problems were detected in the forecast outputs of the model since the model became operational in mid-September 1988.

(b) Governing equations

The governing equations in sigma coordinate, with the x-axis and y-axis parallel to the latitudes and longitudes respectively are :

Equations of motion

$$\frac{\partial}{\partial t}\left(\frac{\pi}{m^2}u\right) = -\frac{\partial}{\partial x}(u^*u) - \frac{\partial}{\partial y}(v^*u) - \frac{\partial}{\partial \sigma}\left(\frac{\pi\dot{\sigma}}{m^2}u\right)$$

$$+\pi v\left\{\frac{f}{m^2} + v\frac{\partial}{\partial x}\left(\frac{1}{m}\right) - u\frac{\partial}{\partial y}\left(\frac{1}{m}\right)\right\} - \frac{\pi}{m}\left\{\frac{\partial \phi}{\partial x} + C_p\,\theta\,\frac{\partial P^{k_a}}{\partial x}\right\}$$

$$+\frac{\pi}{m^2}F_u - \frac{g}{m^2}\left(\frac{\partial \tau}{\partial \sigma}\right)_x \qquad (3.1)$$

$$\frac{\partial}{\partial t}\left(\frac{\pi}{m^2}v\right) = -\frac{\partial}{\partial x}(u^*v) - \frac{\partial}{\partial y}(v^*v) - \frac{\partial}{\partial \sigma}\left(\frac{\pi\dot{\sigma}}{m^2}v\right)$$

$$+\pi u\left\{\frac{f}{m^2} + v\frac{\partial}{\partial x}\left(\frac{1}{m}\right) - u\frac{\partial}{\partial y}\left(\frac{1}{m}\right)\right\} - \frac{\pi}{m}\left\{\frac{\partial \phi}{\partial y} + C_p\,\theta\,\frac{\partial P^{k_a}}{\partial y}\right\}$$

$$+\frac{\pi}{m^2}F_v - \frac{g}{m^2}\left(\frac{\partial \tau}{\partial \sigma}\right)_y \qquad (3.2)$$

Hydrostatic equation

$$\frac{\partial \phi}{\partial \sigma} = -C_p\,\theta\,\frac{\partial P^{k_a}}{\partial \sigma} \qquad (3.3)$$

Continuity equation

$$\frac{\partial}{\partial t}\left(\frac{\pi}{m^2}\right) = -\left(\frac{\partial u^*}{\partial x} + \frac{\partial v^*}{\partial y}\right) - \frac{\partial}{\partial \sigma}\left(\frac{\pi}{m^2}\dot{\sigma}\right) \qquad (3.4)$$

Tendency equation

$$\frac{\partial}{\partial t}\left(\frac{\pi}{m^2}\right) = -\int_0^1 \left(\frac{\partial u^*}{\partial x} + \frac{\partial v^*}{\partial y}\right) d\sigma \qquad (3.5)$$

Thermal equation

$$\frac{\partial}{\partial t}\left(\frac{\pi}{m^2}\theta\right) = -\frac{\partial}{\partial x}(u^*\theta) - \frac{\partial}{\partial y}(v^*\theta) - \frac{\partial}{\partial \sigma}\left(\frac{\pi\dot{\sigma}}{m^2}\theta\right)$$

$$+ \frac{\pi}{m^2}F_\theta + \frac{\pi}{m^2}Q + \frac{q}{C_p}\frac{1}{m^2}\frac{\partial H}{\partial \sigma} \qquad (3.6)$$

Equation of water vapor

$$\frac{\partial}{\partial t}\left(\frac{\pi}{m^2}q\right) = -\frac{\partial}{\partial x}(u^*q) - \frac{\partial}{\partial y}(v^*q) - \frac{\partial}{\partial \sigma}\left(\frac{\pi\dot{\sigma}}{m^2}q\right)$$

$$+ \frac{\pi}{m^2}F_q + \frac{\pi}{m^2}M + \frac{q}{m^2}\frac{\partial E}{\partial \sigma} \qquad (3.7)$$

Gas law

$$\frac{1}{\rho} = -\frac{R_a T}{\pi\sigma + P_t} \qquad (3.8)$$

The continuity equation may be integrated between two sigma levels to obtain the equation (3.9), which is useful in solving the whole equation set :

$$\left(\frac{\pi\dot{\sigma}}{m^2}\right)_{\sigma+\Delta\sigma} = \left(\frac{\pi\dot{\sigma}}{m^2}\right)_{\sigma} - \int_{\sigma}^{\sigma+\Delta\sigma}\frac{\partial}{\partial t}\left(\frac{\pi}{m^2}\right) + \frac{\partial u^*}{\partial x} + \frac{\partial v^*}{\partial y}\, d\sigma \qquad (3.9)$$

The vertical velocity 'ω' and temperature 'T' can be obtained diagnostically from relations (3.10) and (3.11) respectively :

$$\omega = \frac{dp}{dt} = m^2\left\{\sigma\frac{\partial}{\partial t}\left(\frac{\pi}{m^2}\right) + \sigma\left(\frac{u}{m}\frac{\partial \pi}{\partial x} + \frac{v}{m}\frac{\partial \pi}{\partial y}\right) + \frac{\pi\dot{\sigma}}{m^2}\right\} \qquad (3.10)$$

$$T = P^{k_a}\theta \qquad (3.11)$$

In the above equations, $P = p/p_0$, $p_0 = 1000$ hPa, $k_a = R_a/C_p$, $u^* = \frac{\pi}{m} u$ and $v^* = \frac{\pi}{m} v$. R_a, C_p, m are the gas constant of dry air, the specific heat of air at constant pressure and the map factor, respectively. F_u, F_v, F_θ, F_q denote the subgrid-scale horizontal diffusion coefficients for momentum (u and v component), potential temperature and water vapor, respectively. Q and M represent the diabatic heating per unit mass and the moisture source per unit mass respectively.

The horizontal stress vector due to the vertical turbulent flux of horizontal momentum, the vertical turbulent fluxes of heat and moisture are :

$$\underline{\tau} = -\frac{\rho^2 g}{\pi} K_m \frac{\partial \underline{v}}{\partial \sigma} \tag{3.12}$$

$$H = (C_p \rho^2 g/\pi) K_h \frac{\partial \theta}{\partial \sigma} \tag{3.13}$$

$$E = (\rho^2 g/\pi) K_e \frac{\partial q}{\partial \sigma} \tag{3.14}$$

(c) Physical processes in the model

The physical processes included in the model are : flux in the surface layer, radiation, vertical diffusion, large scale condensation, convection and horizontal diffusion.

(i) Fluxes in the surface layer

The Monin-Obukhov similarity theory (Businger et al, 1971) is employed in the computation of surface fluxes. The profiles of variables depend on external parameters and surface fluxes as follows :

$$\frac{kz}{u^*} \frac{\partial |\underline{v}|}{\partial z} = \phi_m \left(\frac{z}{L}\right) \tag{3.15a}$$

$$\frac{kz}{\theta^*} \frac{\partial \theta}{\partial z} = \phi_h \left(\frac{z}{L}\right) \tag{3.15b}$$

$$\frac{kz}{q^*}\frac{\partial q}{\partial z} = \phi_q\left(\frac{z}{L}\right) \tag{3.15c}$$

where k is the Karman's constant. The Monin-Obukhov stability length L is given by :

$$L = -\frac{u_*^3}{k\left(\frac{g}{\theta_{vm}}\right)\overline{w'\theta'}_v} \tag{3.16}$$

where θ_v is the virtual potential temperature, θ_{vm} the mean surface layer virtual potential temperature. The scaling parameter u_*, θ_*, q_* are related to the surface fluxes as follows :

$$\frac{\tau}{\rho} = -\left|\overline{w'v'}\right|_s = u_*^2 \tag{3.17a}$$

$$\frac{H}{\rho C_p} = \left(\overline{w'\theta'}\right)_s = -u_*\theta_* \tag{3.17b}$$

$$\frac{E}{\rho} = \left(\overline{w'q'}\right)_s = -u_*q_* \tag{3.17c}$$

The suffix s denotes the values at the earth's surface. The virtual potential temperature flux is approximately related to the sensible heat and moisture flux as in equation (3.18) :

$$\left(\overline{w'\theta'_v}\right)_s = \left(\overline{w'\theta'}\right)_s + 0.61\,\theta_m\left(\overline{w'q'}\right)_s \tag{3.18}$$

where θ_m is the mean surface layer potential temperature.

The lowest level of the model ($\approx$40 m above the surface) is assumed to lie always within the surface layer and the height of that level is assumed to be z_a.

The bulk Richardson number Ri (which is a function of external parameters) is defined as :

$$Ri = \frac{g z_a \Delta\theta_v}{\theta_{vm}\left|\underline{u}(z_a)\right|^2} \tag{3.19}$$

$$\Delta\theta_v = \Delta\theta + 0.61\,\theta_m\Delta q$$

The surface wind speed is assumed to be more than 0.5 m/sec to avoid computational difficulty.

$$u_*^2 = C_m |u|^2 \tag{3.20a}$$

$$u_* \theta_* = C_h |u| \Delta\theta \tag{3.20b}$$

$$u_* q_* = C_h |u| \Delta q \tag{3.20c}$$

where $C_m = \left(\frac{k}{\ell n \frac{za}{z_o}}\right)^2 f_m \left(Ri, \frac{za}{z_o}\right)$

and $C_h = \left(\frac{k}{\ell n \frac{za}{z_o}}\right)^2 f_h \left(Ri, \frac{za}{z_o}\right)$

The empirical expressions chosen for the unstable case (Ri<o) are :

$$f_h = 1 - \frac{3bRi}{1 + a_h\left(\frac{za}{z_o}\right)\sqrt{-Ri}} \tag{3.21a}$$

$$a_h\left(\frac{za}{z_o}\right) = C \cdot 3b\left[\frac{k}{\ell n\left(\frac{za}{z_o}\right)}\right]^2 \sqrt{\frac{za}{z_o}} \tag{3.21b}$$

$$f_m = 1 - \frac{2bRi}{1 + 3bC\left[\frac{k}{\ell n\left(1 + \frac{za}{z_o}\right)}\right]^2 \sqrt{\left(1 + \frac{za}{z_o}\right)(-Ri)}} \tag{3.21c}$$

where C = 5 and b = 5.

For lack of better information and to minimise the computing time we chose for the whole stable range (Ri>0) the following expressions (d=5);

$$f_m = \frac{1}{1 + 2bRi/\sqrt{1+dRi}} \tag{3.22a}$$

$$f_h = \frac{1}{1 + 3bRi/\sqrt{1+dRi}} \tag{3.22b}$$

Correction for the roughness parameter

The surface values θ_s and q_s are extrapolated assuming logarithmic profiles. Thus the following equations are obtained using the same arguement as Kondo (1975) :

$$\theta(z_a) - \theta_s = \theta_* \left(\frac{u_*}{C_h|u|} + B_h^{-1}\right) \tag{3.23a}$$

$$q(z_a) - q_s = q_* \left(\frac{u_*}{C_h|u|} + B_e^{-1}\right) \tag{3.23a}$$

Kondo (1975) suggests the following approximation formulae for the correction factors B_h^{-1} and B_e^{-1} :

Over sea,

$$B_h^{-1} = \frac{1}{k} \ell n \left(\frac{\nu + ku_* z_0}{\sigma}\right) \tag{3.24a}$$

$$B_e^{-1} = \frac{1}{k} \ell n \left(\frac{\nu + ku_* z_0}{D}\right) \tag{3.24b}$$

Over land,

$$B_h^{-1} = 0.47 \left(\frac{15u_* z_0}{\nu}\right)^{0.45} \tag{3.25a}$$

$$B_e^{-1} = 0.54 \left(\frac{15u_* z_0}{\nu}\right)^{0.45} \tag{3.25b}$$

where α is the thermal conductivity of air, ν the kinetic viscosity of air and D the molecular diffusion coefficient of air. In this model, the same formulae are used for B_h^{-1} and B_e^{-1} over the sea. However, B_h^{-1} and B_e^{-1} are assumed to be zero over land.

Roughness parameter over the sea

The sea surface temperature is assumed constant and the roughness parameter assumed to depend only on the surface wind speed. We use the following relations between roughness parameter and friction velocity :

$$z_0 = (-34.7 + 8.28\, u_*) \times 10^{-4} \qquad u_{10} \leqq 25 \text{ m/s} \tag{3.26a}$$

$$z_0 = -0.277 + 3.39 \times 10^{-3}\, u_* \qquad u_{10} > 25 \text{ m/s} \tag{3.26b}$$

where u_{10} the wind speed at 10 m height above the sea level. These expressions are approximated from the relation derived from the formula given in Table A1 of Kondo (1975).

Ground surface temperature

Over land, roughness parameter can be assumed constant and surface temperature depends only on surface fluxes. In this model, the ground surface temperature is computed by Bhumralkar's formula (1975) :

$$\frac{\partial T_g}{\partial t} = -\frac{2\sqrt{\pi}}{\rho_g C_g \sqrt{\nu_g \tau_1}} H_f - \frac{2\pi}{1}(T_g - T_G) \tag{3.27}$$

where $H_f = \varepsilon_g \sigma T_g^4 + \rho C_p (\overline{w'\theta'})_s + L_v (\overline{w'q'})_s - RS(1\text{-}ALBD) - F_\ell$

T_g is the ground surface temperature, ρ_g the soil density, C_g the soil specific heat, ν_g the soil thermal diffusivity, τ_1 a period of one day, T_G a constant deep soil temperature, ε_g the emissivity of the ground surface in the infrared, σ the Stefan-Boltzman constant, L_v the latent heat of water vapor, RS the solar radiation reaching the ground, ALBD the albedo of the ground surface and F_ℓ the downward long wave radiation at the ground surface. Evaporation from the ground surface is computed empirically from

$$(w'q')_s = \beta C_h \left|\underline{v}(z_a)\right| \left(q^*(T_g) - q(z_a)\right) \tag{3.28}$$

where $q^*(T_g)$ is the saturation specific humidity at temperature T_g, β (=0.1) is the parameter specifying the ground wetness and C_h the bulk transfer coefficient.

(ii) Parameterization of radiation

A simplified parameterization scheme is adopted for the radiation process in the model. Only solar radiation and downward long wave radiation are computed. The terms RS and F_ℓ are expressed by the following empirical formulae :

$$RS = S_0(1 - cl.CL)\ (1 - cm.CM)\ (1 - ch.CH) \tag{3.29}$$

$$S_0 = (TAU)\ S_\infty \cos\zeta$$

$$(TAU) = a + b \times 10^{-0.13 \sec\zeta} \tag{3.30}$$

where $b = 0.43 + 0.016\ e_a$

and $a = 1 - b - 0.06 \log_{10} e_a$

where S_∞ is the solar constant, ζ the zenith angle, e_a the water vapor pressure near the ground surface. CL, CM and CH are the amount of low, medium and high cloud, respectively. They are calculated using the relative humidity at levels 4 and 5 (for low cloud), 7 and 8 (for medium cloud) and levels 10 and 11 (for high cloud) by the empirical formula (Smagorinsky, 1960). Magnitudes of cl, cm and ch which represent the effect of absorption and reflection by cloud are 0.7, 0.6, 0.3, respectively. The empirical formula (3.30) is proposed by Kondo (1976).

Downward long wave radiation is approximated by Brunt's formula, taking into consideration the effect of cloud,

$$\frac{F_\ell}{\varepsilon_g T_a^4} = \left\{ 1 - (0.49 - 0.066\sqrt{e_a}) \right\} (1 - C.A) \tag{3.31}$$

T_a is the screen level temperature which is assumed to be the lowest level temperature in the model. Kondo (1975) had given expressions for the correction factors C and A :

$$C = 0.75 - 0.005\ e_a \tag{3.32a}$$

$$A = CL + 0.85CM + 0.5CH \tag{3.32b}$$

(iii) Vertical turbulent diffusion above the surface layer

The level 2 version of the closure model proposed by Mellor and Yamada (1974) is employed in this model to estimate the vertical turbulent diffusion above the surface layer

$$\left(\frac{\tau}{\rho}\right)_x = -\overline{u'w'} = K_m \frac{\partial u}{\partial z} \tag{3.33a}$$

$$\left(\frac{\tau}{\rho}\right)_y = -\overline{v'w'} = K_m \frac{\partial v}{\partial z} \tag{3.33b}$$

$$\frac{H}{\rho C_p} = \overline{\theta'w'} = -K_h \frac{\partial \theta}{\partial z} \tag{3.33c}$$

$$\frac{E}{\rho} = \overline{q'w'} = -K_h \frac{\partial q}{\partial z} \tag{3.33d}$$

where $K_m = \ell^2 \frac{\partial V}{\partial z} S_m$

$$K_h = \ell^2 \frac{\partial V}{\partial z} S_h$$

The terms S_m and S_h are calculated from the flux Richardson number, Rf, as

$$S_m = B_1^{1/2} (1 - Rf)^{1/2} (\tilde{S}_m)^{3/2} \qquad Rf < Rf_c = 0.213 \tag{3.34a}$$

$$S_h = B_1^{1/2} (1 - Rf)^{1/2} (\tilde{S}_m)^{1/2} \tilde{S}_h$$

$$S_m = S_h = 0 \qquad Rf \geq Rf_c \tag{3.34b}$$

B_1 is a constant. S_m and S_h are functions of the flux Richardson number. The length scale ℓ is given by

$$\ell = \frac{kz}{1 + kz/\ell_0} \tag{3.35}$$

where $\ell_0 = 0.10 \dfrac{\int_0^\infty bz\,dz}{\int_0^\infty b\,dz}$

$$b^2 = \overline{u'^2} + \overline{v'^2} + \overline{w'^2}$$

The turbulent intensity represents the dissipation due to the transfer of energy from the mean flow and the generation due to buoyancy as

$$\frac{b^3}{15\ell} = -\overline{u'w'}\frac{\partial u}{\partial x} - \overline{v'w'}\frac{\partial v}{\partial y} + \frac{g}{\theta_v}\overline{w'\theta'_v} \qquad (3.36)$$

The above turbulent diffusion process is applied to all levels of the model above the surface layer.

(iv) Large scale condensation

Latent heating is mainly due to large scale condensation or condensation in deep cumulus convection. Large scale condensation occurs whenever q exceeds its saturation value q_s at temperature T, giving rise to the release of latent heat. The supply of latent heat increases the temperature as well as the saturation value. At the same time, q decreases due to condensation. A stage is eventually reached when the temperature increases to $T + \delta T$ and q equals q'_s, the new saturation value of the specific humidity at temperature $T + \delta T$. Then condensation stops, ending the release of latent heat. Now

$$\delta T = \frac{L}{c_p}(q - q_s) \ , \qquad (3.37)$$

$$q'_s = q_s + \frac{\partial q_s}{\partial T}\delta T \ , \qquad (3.38)$$

and by Clausius Clapeyron's theorem

$$\frac{\partial q_s}{\partial t} \doteq \frac{L q_s}{R_v T^2} \ , \qquad (3.39)$$

where L is the latent heat of evaporation of water and R_v the gas constant for moist air. Elimination of $\frac{\partial q_s}{\partial T}$ and q_s' from equations (3.37) to (3.39) gives the total latent heat released due to large scale precipitation Q :

$$Q = c_p \frac{\delta T}{\delta t} = \frac{L(q - q_s)}{\delta t \left(1 + \frac{L^2 q_s}{c_p R_v T^2} \right)} \quad , \tag{3.40}$$

q_s can be calculated from

$$q_s = \frac{0.622\ e_s}{p} \quad , \tag{3.41}$$

The saturation vapour pressure of water vapour is given by

$$e_s = 6.11 \exp\{ 25.22\ (1 - \tfrac{273}{T}) \}\ (\tfrac{273}{T})^{5.31} \tag{3.42}$$

In this model, condensed moisture is assumed to fall down to ground as precipitation without evaporation.

(v) Parameterization of convection

The parameterization scheme for convection used in this model is of the moist convective adjustment type similar to that proposed by Gadd and Keers (1970). Convection is assumed to occur whenever the lapse rate is larger than some pre-defined critical value Γ_c given by

$$\Gamma_c = \frac{1}{1 - U_c} \{ \Gamma_d\ (1-U) + \Gamma_m\ (U-U_c) \} \tag{3.43}$$

where Γ_d is the dry adiabatic lapse rate, Γ_m the moist adiabatic lapse rate, U the relative humidity and U_c the critical relative humidity taken as 0.5 in this model. In such circumstances, the temperature and moisture are adjusted in such a way that the resultant lapse rate become Γ_c subject to the condition that the relative humidity remains the same during the adjustment process. Excess moisture after the adjustment is assumed to reach the ground as precipitation without evaporation. This adjustment process is applied from level 4 upwards.

(vi) Horizontal diffusion

The horizontal diffusion terms F_u, F_v, F_θ and F_q are given empirically as fourth-order Laplacians with constant diffusion coefficients :

$$F_u = - K_H \nabla \cdot \{\pi \nabla (\nabla_+^2 u)\} - K_{div} \pi \frac{\partial}{\partial x} \{\nabla_+^2 (\nabla . \underline{v})\} \quad (3.44)$$

$$F_v = - K_H \nabla \cdot \{\pi \nabla (\nabla_+^2 v)\} - K_{div} \pi \frac{\partial}{\partial y} \{\nabla_+^2 (\nabla . \underline{v})\} \quad (3.45)$$

$$F_\theta = - K_H \nabla \cdot \{\pi \nabla (\nabla_+^2 \theta)\} \quad (3.46)$$

$$F_q = - K_H \nabla \cdot \{\pi \nabla (\nabla_+^2 q)\} \quad (3.47)$$

where ∇_+^2 is a non-dimensional Laplacian operator defined by

$$\nabla_+^2 X\ (x,y) = X(x+d,y) + X(x-d,y) + X(x,y+d) + X(x,y-d) - 4X(x,y) \quad (3.48)$$

The diffusion coefficients K_H and K_{div} used in the model are

$$K_H = K_{div} = 10^5\ m^2/sec$$

where d is the grid length. These diffusion terms are evaluated on sigma-surfaces.

Each momentum equation contains two diffusion terms. The first term is the same as those in the thermodynamic and water vapor equations, and it acts on both the rotational and the divergent component of u and v. It is interesting to note that when the momentum equations are converted to the vorticity and the divergence equations assuming that π is constant, the diffusion terms become

$$\frac{\partial \zeta}{\partial t} = ... - K_H \nabla^2 (\nabla_+^2 \zeta) \quad (3.49a)$$

$$\frac{\partial D}{\partial t} = ... - (K_H + K_{div}) \nabla^2 (\nabla_+^2 D) \quad (3.49b)$$

where ζ ($= k \cdot \nabla x \underline{v}$) is vorticity and D ($= \nabla \cdot \underline{v}$) the divergence.

(d) Topography

As the domain of the RO limited area model is different from that of the JMA VFM65, a new topography has to be constructed. In designing our topography, we have to bear in mind that the lateral boundary data come from the JMA Global Spectral Model. In order to avoid the generation of inertial waves due to discontinuity across the boundary, the topography field employed in our model should be one that could be joined smoothly with that of the JMA model in the lateral boundary region (Figure 5).

Our first attempt was to adapt the topography field of the JMA Global Spectral Model which is computed by converting 10 minute latitude/longitude resolution grid-point topography values as read from relief map to spherical harmonics truncated at wavenumber 63. These harmonics are then smoothed by using the following exponential filter (Hoskins, 1980) :

$$(\Phi^m_{s_n}) \text{ smoothed} = \Phi^m_{s_n} \exp\,(-kn^2/n+1)^2 \qquad (3.50)$$

where $k = 0.7 \times 10^{-6}$. The grid-point resolution of the global topography field is 1.875 degree. A bicubic spline is employed to interpolate this field into a one degree resolution field (TG) for use in our model. The resultant field is too smooth for a one degree resolution model. The Nanling ridge, which plays an important role in controlling the flow of the northerly airstream over South China, is not accurately represented (Figure 6). Operational experience showed that the model with this topography did not perform well in respect of the timing of the arrival of surges of winter monsoon to Hong Kong.

Currently, the model employs an envelope topography (TE) with one standard deviation, derived from the 10 minute latitude/longitude resolution grid-point topography data. The resulting field is much more realistic (Figure 7). However, the problem of 'smooth transition in the boundary region' still exists and inertial waves were suspected to occur in the in-coming boundary occasionally. Further numerical experimentation will be carried out for a new topography (T) = K_B (TG) + (1-K_B) (TE), where

$$K_B = k_B\left(\frac{L_B - \ell}{L_B}\right)^{\beta} \quad , \quad 0 < \ell < L_B$$

$$K_B = 0 \quad , \quad L_B \leq \ell$$

L_B stands for the width of the boundary region and ℓ the distance from the lateral boundary (Figure 8).

(e) Initialization

The mean sea level pressure, wind, temperature and height at the ten pressure levels and the dew-point depression at the four pressure levels analysed by the operational optimal interpolation data analysis scheme are vertically interpolated to the thirteen sigma levels using cubic spline. The specific humidity is computed from the dew-point depression and temperature. It is then modified to eliminate supersaturation and instability. A nine-point filter was applied to all variables on the sigma levels to remove horizontal two-grid waves.

Numerical experimentations have been carried out on dynamic initialization schemes proposed by Sugi (1986) using the following as the forward-backward integration schemes :

(i) Tatsumi's economic explicit scheme (Figure 9);

(ii) Okamura scheme.

However, the schemes failed to converge after a considerable number of iterations. As an interim measure, therefore, the limited area model is now integrated operationally without the use of any initialization scheme.

According to Satomura (1988), implicit schemes will be more effective as the forward-backward integration scheme in dynamic normal mode initialization. Considerations are being given to developing a dynamic initialization scheme to improve the performance of the limited area model.

(f) Time integration scheme

The Tatsumi's (1983) economical explicit scheme is employed to integrate the RO limited area model forward in time. The flow of this scheme is shown in Figure 9. The main feature of this scheme is the introduction of two time steps : the longer main time step Δt_a and the shorter sub-time step Δt_b. The length of the main time step is limited by the wind speed and varies from 6 to 15 minutes. It is checked every 3 hour and adjusted when necessary. Thus the main time step is 4-8 times longer than that of the usual leap-frog scheme, resulting in less integration steps required. According to Tatsumi (1983), the computation time for a 48 hour forecast will be reduced to half of that by the leap-frog scheme.

Time tendencies of all variables are computed at every main time step. In order to maintain numerical stability for high frequency gravity wave oscillations, these time tendencies are modified (within the main time step) by re-computing only those terms which are responsible for gravity wave generation at every sub-time step.

The governing equations for the integration at sub-time steps can be written as

$$\frac{\partial \underline{v}'}{\partial \tau} = \left(\frac{\partial \underline{v}}{\partial t}\right)^n - \nabla \phi' - \sigma \alpha^n \nabla \pi' \tag{3.51a}$$

$$\frac{\partial \theta'}{\partial \tau} = \left(\frac{\partial \theta}{\partial t}\right)^n - \dot{\sigma}' \frac{\partial \theta^n}{\partial \sigma} \tag{3.51b}$$

$$\frac{\partial q'}{\partial \tau} = \left(\frac{\partial q}{\partial t}\right)^n \tag{3.51c}$$

$$\frac{\partial \pi'}{\partial \tau} = \left(\frac{\partial \pi}{\partial t}\right)^n - \pi^n \int_0^1 \nabla \cdot \underline{v}' d\sigma \tag{3.51d}$$

$$\dot{\sigma}' = -\int_0^\sigma \nabla \cdot \underline{v}' d\sigma + \int_0^1 \nabla \cdot \underline{v}' d\sigma \tag{3.51e}$$

$$\frac{\partial \phi'}{\partial \sigma} = -\alpha^n \left\{1 + (\kappa - 1)\frac{\pi^n \sigma}{p^n}\right\}\pi' - \frac{\alpha^n \pi^n}{\theta^n}\theta' \tag{3.51f}$$

$(\partial X/\partial t)^n$ ($X : \pi$, u, v, θ, q) is calculated by the finite difference analogue of the governing equations (3.1) to (3.11) using the values defined at the nth time step and the relation

$$\frac{\partial}{\partial t}\left(\frac{\pi}{m^2} X\right) = \frac{\pi}{m^2}\frac{\partial X}{\partial t} + X\frac{\partial}{\partial t}\left(\frac{\pi}{m^2}\right) \tag{3.52}$$

The variable τ is the time relative to the nth time step which is defined between n-1 and n+1 time step ($-\Delta t_a \leqslant \tau \leqslant \Delta t_a$). The perturbation variable X' (X' stands for π', u', v', or q') in equations (3.51a) to (3.51f) is defined as

$$X'(\tau) = X(\tau) - X^n$$

$$X'(-\Delta t_a) = X^{n-1} - X^n$$

$$X^{n+1} = X^n + X'(\Delta t_a)$$

Finite difference formulation of the perturbation terms in (3.51a) to (3.51f) are defined as follows :

$$\nabla \phi' = \bar{m}\left\{\overline{\delta x \phi'}^{y} , \overline{\delta y \phi'}^{x}\right\} \tag{3.53a}$$

$$\nabla \pi = \bar{m}\left\{\overline{\delta x \pi'}^{y} , \overline{\delta y \pi'}^{x}\right\} \tag{3.53b}$$

$$\nabla \cdot \underline{v}' = m^2\left\{\overline{\delta x (u'/\bar{m})}^{y} + \overline{\delta y (v'/\bar{m})}^{x}\right\} \tag{3.53c}$$

where $\nabla\phi'$ and $\nabla\pi'$ are defined on the vector point, $\nabla \cdot \underline{v}'$ at scalar point.

The operators δ_x, δ_y, $\overline{}^{x}$, $\overline{}^{y}$, $\overline{}$ are

$$\delta_x X(x,y) = \frac{1}{d}\left\{X(x + \frac{d}{2}, y) - X(x - \frac{d}{2}, y)\right\} \tag{3.54a}$$

$$\delta_y X(x,y) = \frac{1}{d}\left\{X(x,y + \frac{d}{2}) - X(x,y - \frac{d}{2})\right\} \tag{3.54b}$$

$$\overline{X(x,y)}^{x} = \frac{1}{2}\left\{X(x + \frac{d}{2}, y) + X(x - \frac{d}{2}, y)\right\} \tag{3.54c}$$

$$\overline{X(x,y)}^{y} = \frac{1}{2}\left\{X(x,y + \frac{d}{2}) + X(x,y - \frac{d}{2})\right\} \tag{3.54d}$$

$$\overline{X(x,y)} = \frac{1}{4}\left\{X(x + \frac{d}{2}, y + \frac{d}{2}) + X(x - \frac{d}{2}, y + \frac{d}{2}) + X(x + \frac{d}{2}, y - \frac{d}{2}) + X(x - \frac{d}{2}, y - \frac{d}{2})\right\} \tag{3.54e}$$

Vertical difference operators in (3.51a) to (3.51f) are evaluated in the following way by using the level suffix k

k = 1 : lower boundary
k = 2K+1 : upper boundary
} where $\dot{\sigma} = 0$

even k : u, v, θ, q, ... level

odd k : $\dot{\sigma}$ level

Variables are arranged on the levels in the following way :

even number level : $\underline{v}'$, θ', ϕ', θ^n, A^n, B^n,

odd number level : $\dot{\sigma}'$ $\hat{\phi}'$

where A^n, B^n, and $\Delta\sigma$ are given by

$$A^n = -\alpha^n \left(1 + (K-1)\frac{\pi^n \sigma}{p^n}\right) \tag{3.55a}$$

$$B^n = -\alpha^n \pi^n / \theta^n \tag{3.55b}$$

$$\Delta\sigma_k = \sigma_{k-1} - \sigma_{k+1} \tag{3.55c}$$

For the vertical integration of $\nabla \cdot \underline{v}'$:

$$\int_0^{\sigma_L} \nabla \cdot \underline{v}' d\sigma = \sum_{k = 3, 5, \ldots, L} (\nabla \cdot \underline{v}'_k) \cdot \Delta\sigma_k \tag{3.56}$$

For the vertical advection of potential temperature :

$$\left(\dot{\sigma}' \frac{\partial \theta^n}{\partial \sigma}\right)_k = \begin{cases} \dfrac{1}{2\Delta\sigma_k} \dot{\sigma}'_{k+1} \left(\theta^n_k - \theta^n_{k+2}\right) & (k = 2) \\ \dfrac{1}{2\Delta\sigma_k} \left\{\dot{\sigma}'_{k+1} \left(\theta^n_k - \theta^n_{k+2}\right) + \dot{\sigma}'_{k-1} \left(\theta^n_{k-2} - \theta^n_k\right)\right\} & (k = 4, 6, \ldots 2K-2) \\ \dfrac{1}{2\Delta\sigma_k} \dot{\sigma}'_{k-1} \left(\theta^n_{k-2} - \theta^n_k\right) & (k = 2K) \end{cases} \tag{3.57}$$

For the hydrostatic equation :

$$\begin{aligned} &\frac{\hat{\phi}'_{k-1} - \hat{\phi}'_{k+1}}{\Delta\sigma_k} = A^n_k \pi' + B^n_k \theta'_k \qquad (k=2,4,\ldots,2K) \\ &\phi'_k = (\hat{\phi}'_{k+1} + \hat{\phi}'_{k-1})/2 \end{aligned} \tag{3.58}$$

where $\hat{\phi}'_1 = 0$.

The convergence of the Tatsumi scheme is not strong enough. This necessitates the introduction of more damping schemes into the model. At present, the modified version of the Asselin (1972) time filter and the gravity wave damping scheme are used with the damping parameters set to 0.1 in both schemes.

(g) Lateral boundary condition

The formulation of the lateral boundary condition follows that proposed by Hovermale (unpublished).

In the boundary region which is 7 grids in width from the lateral boundary (the dotted area in Figure 9), the following terms are added to the momentum, thermodynamic and tendency equations.

$$\frac{\partial}{\partial t}\left(\frac{\pi}{m^2}X\right) = \cdots\cdots + K_B \frac{\pi}{m^2} \nabla_x^2 (X - X_{HSM}) \tag{3.59a}$$

$$\frac{\partial}{\partial t}\left(\frac{\pi}{m^2}\right) = \cdots\cdots + K_B \frac{1}{m^2} \nabla_x^2 (\pi - \pi_{HSM}) \tag{3.59b}$$

where

$$K_B = k_B \frac{L_B - \ell}{L_B}^{\beta}, \quad 0 < \ell < L_B$$

$$K_B = 0, \quad L_B \leq \ell$$

The variable X stands for u, v, θ or q. X_{HSM} and π_{HSM} are supplied externally. L_B is the width of the boundary region and ℓ the distance from the lateral boundary.

In this model,

$$k_B = 4 \times 10^{-4} \text{ sec}^{-1}$$

$$= 1.5$$

$$L_B = 6d \quad (d : \text{grid distance})$$

The operator ∇_X^2 is a non-dimensional finite difference analogue of the Laplacian operator and is defined by

$$\nabla_X^2 X(x,y) = X(x+d, y+d) + X(x+d, y-d) + X(x-d, y+d) + X(x-d, y-d) - 4X(x,y) \tag{3.60}$$

where (x, y) represents Cartesian coordinates of the forecast area and d is the grid distance. At the grid points on the lateral boundary the ∇_X^2 operator cannot be evaluated so that all prognostic variables π, u, v, θ and q have to be set equal to the corresponding forecast values supplied externally.

4. SOME APPLICATION OF THE SYSTEM AROUND HONG KONG

Operationally, forecast surface pressure, upper air streamline and 6-hourly accumulated rainfall charts up to 72 hours are produced once daily. For easy interpretation, forecast tephigram and time cross-section at two grid-points near Hong Kong are also produced. The following is an account of the performance of the model around Hong Kong according to a 1-month data sample (17 Nov - 15 Dec 1988).

4.1 Forecast of Surface Pressure and Temperature

The forecast surface pressure was generally within 2 hPa (Figure 10). The forecast surface temperature was not very accurate. However, the forecast trend was still a useful forecasting aid. In most cases, the forecast overnight temperature drop from the afternoon maximum were smaller than the actual value (Figure 11). Also, most of the forecast changes in morning minimum temperature are in the right categories (Figure 12). When applying this to the forecast of surges of winter monsoon, it was found that the model failed under two circumstances :

(a) on the arrival of northerly surge during fine days, the slight initial temperature rise before the main temperature falls could not be predicted; and

(b) when the surge arrived overnight, the forecast temperature drop in the morning was usually too large.

4.2 Winter Monsoon Surges

The forecast temperature sequence was useful in the forecast of surges of winter monsoon. The timing of the first arrival of surges, was found to be correct in 2 cases out of 5. For the remaining 3 cases, the timings were all 12 hours too early. These cases occurred when the smooth topography was in use. The bias has been reduced after a more realistic Nanling was introduced into the model. Replenishment of cold air was accurately indicated in 7 cases out of 7, which resulted in colder mornings to follow. The first warming-up after a surge was predicted in 4 cases out of 5.

For 850 hPa level, the change from northerly to southerly flow was predicted in 3 cases out of 5. In the remaining 2 cases, the changes were also predicted but with delays of 6 and 12 hours respectively.

4.3 Changes in vertical profile

On several occasions, the model managed to forecast sudden drying up on the 850/700 hPa levels which was not evident from the synoptic pattern, and which would pose considerable problems for forecasters (Figure 13). In general, the timing for the moistening up or drying up of the vertical profile was accurate to within 6 hours.

The verification of the model forecasts for monsoon trough and meso-scale features will be reported separately.

5. CONCLUSIONS

A numerical analysis-forecasting system has been developed for application in Hong Kong. The system consists of two components : a two dimensional multivariate optimal interpolation scheme and a limited area model. These components are the results of adapting the Japan Meteorological Agency optimal interpolation scheme and the very fine mesh limited area model.

The major changes made during the adaptation are :

(a) the use of statistic coefficients that are relevant to the Royal Observatory model domain for the analysis of pressure/height and temperature;

(b) the introduction of a simplied scheme for the generation of bogus data for tropical cyclone;

(c) the replacement of the JMA topography by one which is more relevant to the forecasting requirements in Hong Kong.

Operational forecasters consider that the system has been a useful forecasting tool. The performance of the system according to a 1-month data sample also shows that the model outputs have been reasonable.

6. ACKNOWLEDGEMENT

I would like to express my gratitude to the Directorate of the Royal Observatory for providing me the opportunity to be trained in numerical weather prediction in the European Centre for Medium Range Weather Forecasts and the Japan Meteorological Agency.

I would like to thank Dr. Yukio Kikuchi, Director-General of the Japan Meteorological Agency for supplying the software for the optimal interpolation data analysis scheme and the very fine mesh limited area model to the Royal Observatory for adaptation, as well as for transmitting the boundary data for daily operational runs of the models.

I am also grateful to Dr. H.K. Lam and Mr. C.Y. Lam of the Royal Observatory for their constant advice and encouragement.

Thanks are also due to Miss Kitty Chu for her excellent typing, and to Miss May Wai for her beautiful diagrams.

REFERENCES

1.	Alaka, M.A. and R.C. Elvander	1972	Optimal interpolation from observation of mixed quality. Mon. Weath. Rev., 100,612-624.
2.	Anderson, E. and A. Hollingsworth	1988	Typhoon bogus observations in the ECMWF data assimilation system. ECMWF Res. Dept. Tech. Memorandum No. 148.
3.	Asselin, R.	1972	Frequency filter for time integrations. Mon. Weath. Rev., 100, 487-490.
4.	Bergman, K.H.	1979	Multivariate analysis of temperatures and winds using optimum interpolation. Mon. Weath. Rev., 107, 1423-1444.
5.	Bhumralkar, C.M.	1975	Numerical experiments on the computation of ground surface temperature in an atmospheric general circulation model. J. Appl. Met., 14, 1246-1258.
6.	Businger, J.A., J.C. Wyngaard, Y. Izumi and E.F. Bradley	1971	Flux profile relationships in the atmospheric surface layer. J. Atmos. Sci., 28, 181-189.
7.	Chan, Y.K.	1988	A Manual of the Royal Observatory Numerical Analysis-Forecasting System. ROHK Sectional Note.
8.	Gadd, A.J. and J.F. Keers	1970	Surface exchanges of sensible and latent heat in a 10-level model atmosphere. Quart. J. R. Met. Soc., 96, 297-308.
9.	Hoskins, B.J.	1980	Representation of the earth's topography using spectral harmonics. Mon. Weath. Rev., 108, 111-115.
10.	Japan Meteorological Agency (JMA)	1986	Appendix, 93 pp. Progress report on numerical weather prediction.
11.	Kondo, J.	1975	Air-sea bulk transfer coefficients in diabatic conditions. Bound. Layer Met., 9, 91-112.
12.	Kondo, J.	1976	Heat balance of the East China Sea during the air mass transformation experiment. J. Met. Soc. Japan, 54, 382-398.

13. Kurihara, Y. 1961 Accuracy of winds-aloft data and estimation of error in numerical analysis of atmospheric motions. J. Met. Soc. Japan, Vol. 39, No. 4, 331-343.

14. Lenhard, R.W. 1970 Accuracy of radiosonde temperature and pressure height determination. Bull. Amer. Met. Soc., 51, 842-846.

15. Mellor, G.L. and T. Yamada 1974 A hierarchy of turbulence closure models for planetary boundary layers. J. Atmos. Sci., 31, 1791-1806.

16. Satomura, T. 1988 Dynamic Normal Mode Initialization for a limited-area model. J. Met. Soc. Japan, Vol. 66, No. 3, 261-276.

17. Schlatter, T.W. 1975 Some experiments with a multivariate statistical objective analysis scheme. Mon. Weath. Rev., 103, 246-257.

18. Smagorinsky, J. 1960 On the dynamical prediction of large scale condensation by numerical methods. Geophysical Monographs No. 5, American Geophysical Union, 71-78.

19. Sugi, M. 1986 Dynamic Normal Mode Initialization. J. Met. Soc. Japan, vol. 64, No. 5, 623-636.

20. Tatsumi, Y. 1983 An economical explicit time integration scheme for primitive model. J. Met. Soc. Japan, 61, 269-288.

21. Ueno, M. 1989 Operational bogussing and numerical prediction of typhoon in JMA. JMA/NPD Tech. Rep. No. 28.

100 hPa	———	z, u, v, T
150	———	z, u, v, T
200	———	z, u, v, T
250	———	z, u, v, T
300	———	z, u, v, T
400	———	z, u, v, T, T-Td
500	———	z, u, v, T, T-Td
700	———	z, u, v, T, T-Td
850	———	z, u, v, T, T-Td
Surface	———	p, u, v, T, T-Td

Figure 1 Vertical levels in the Royal Observatory analysis scheme

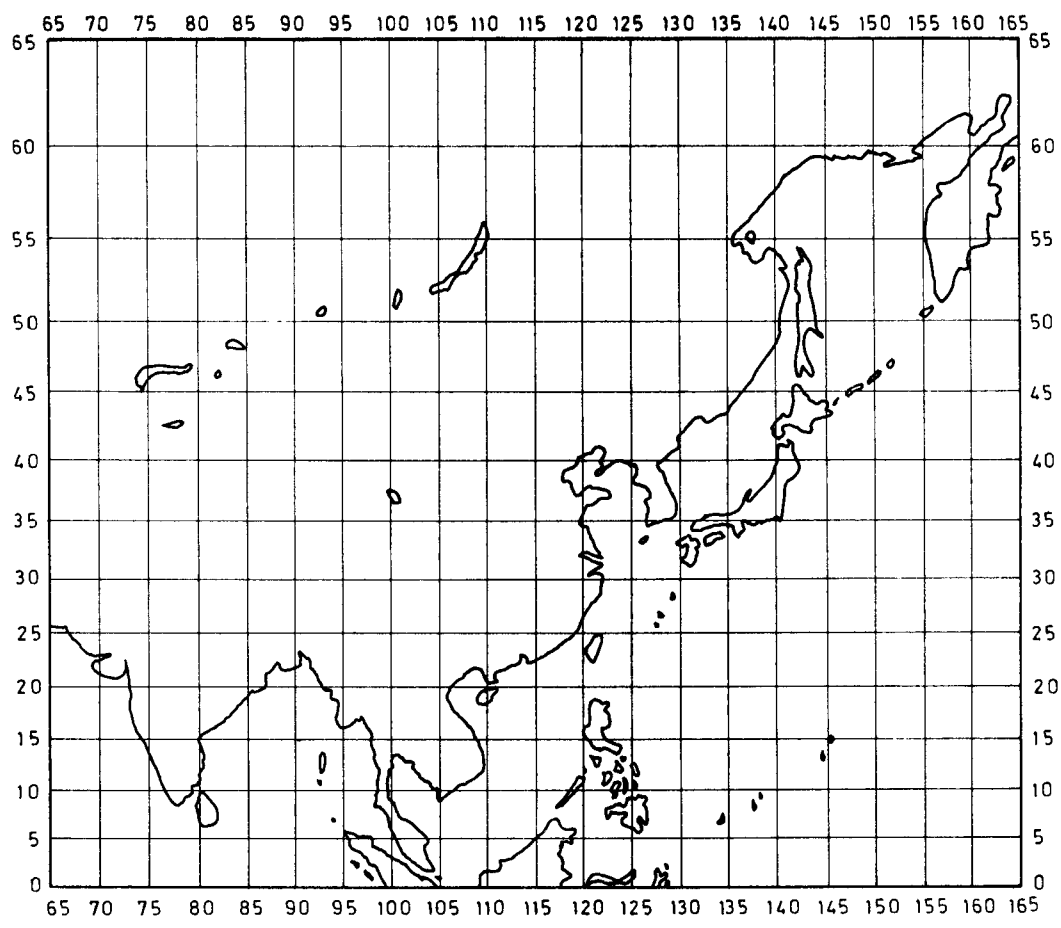

Figure 2 Horizontal domain of the Royal Observatory analysis scheme

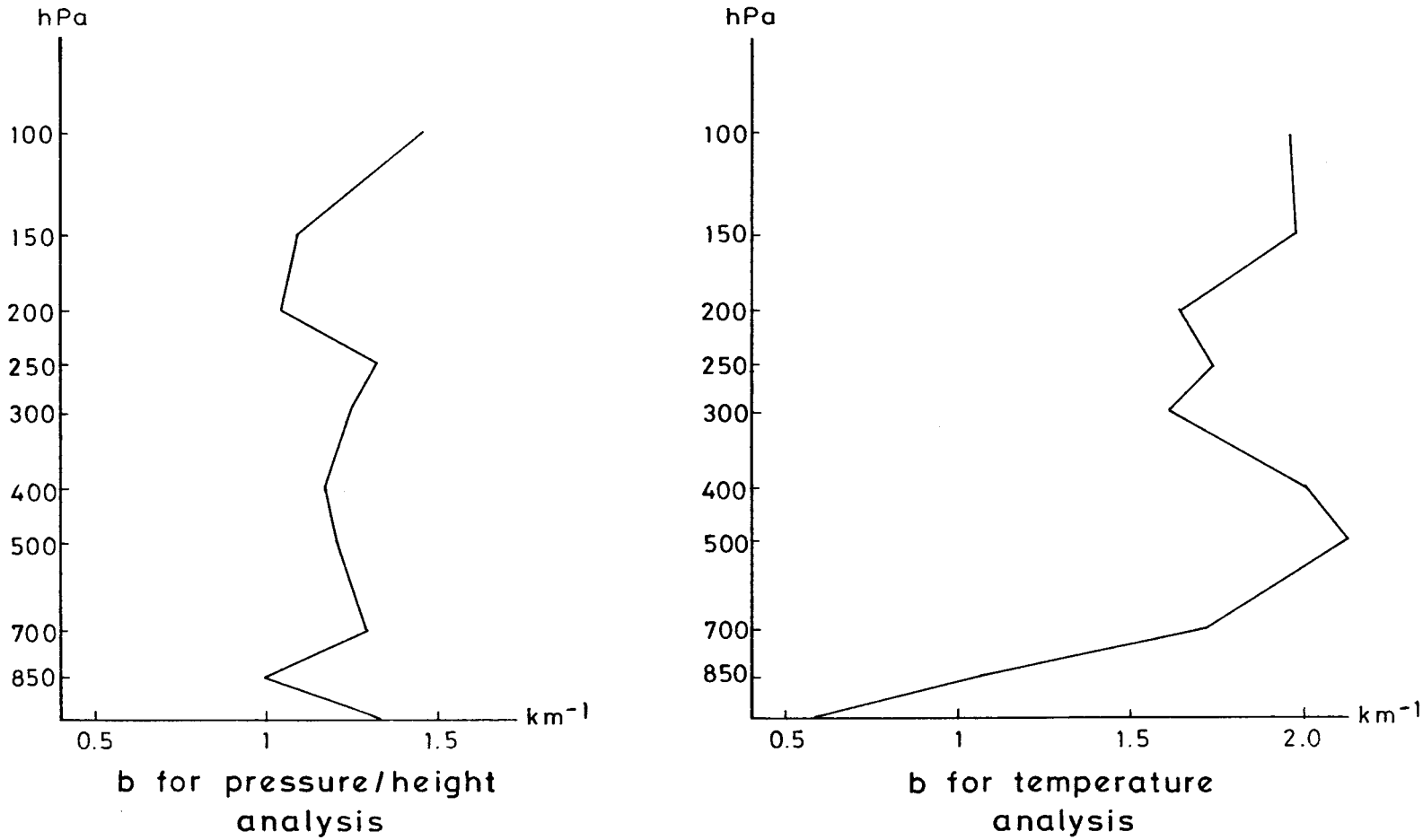

Figure 3 The value of b in equation (2.3)

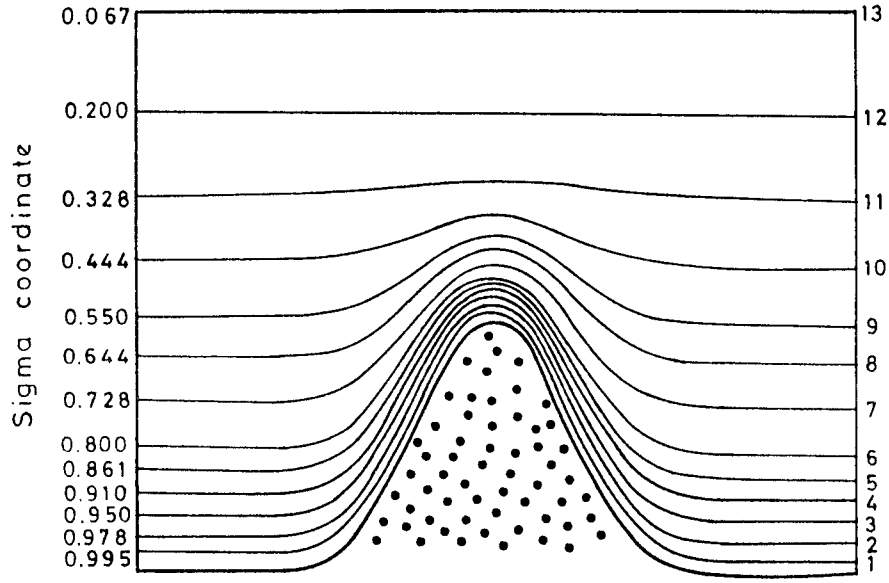

Figure 4 Vertical structure of the Royal Observatory limited area model

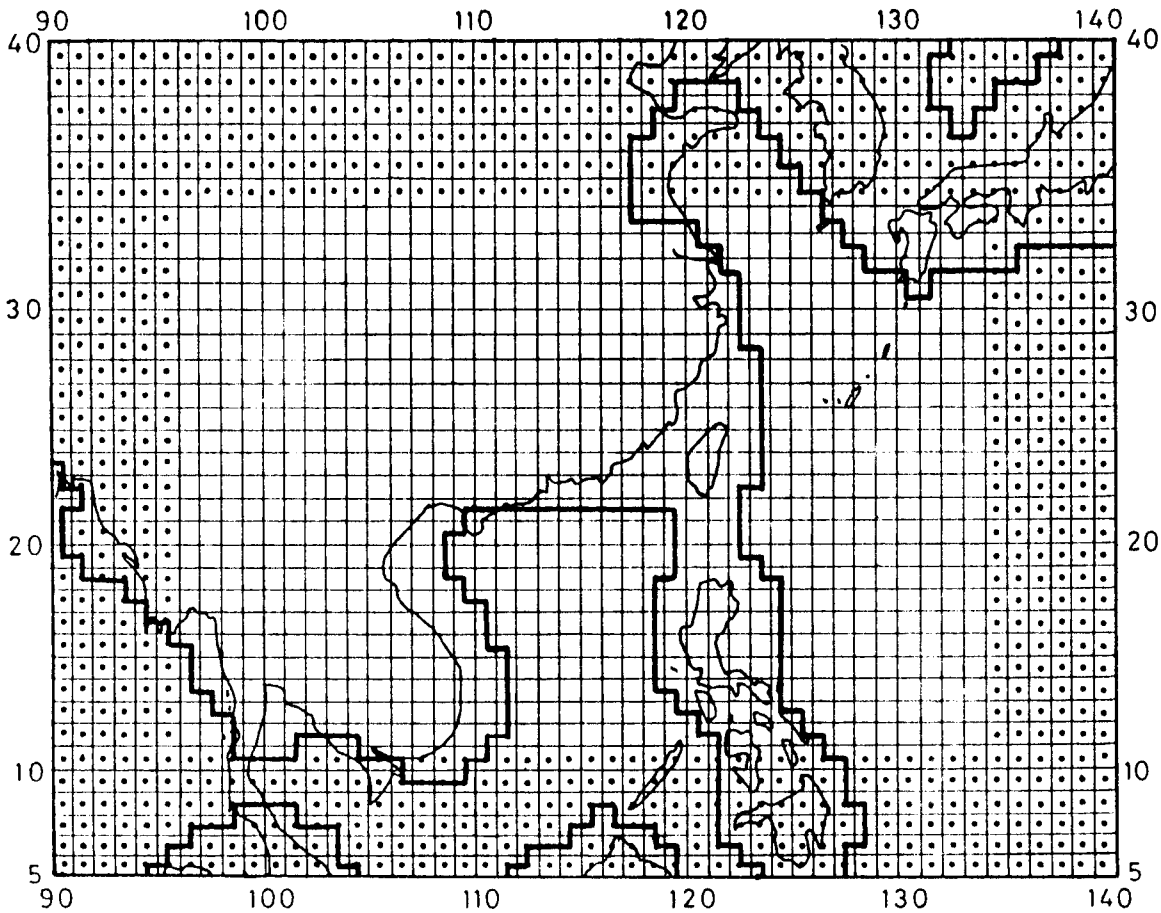

Figure 5 Horizontal domain of the Royal Observatory limited area model. The bold line is the model coastline. The dotted region is the lateral boundary region.

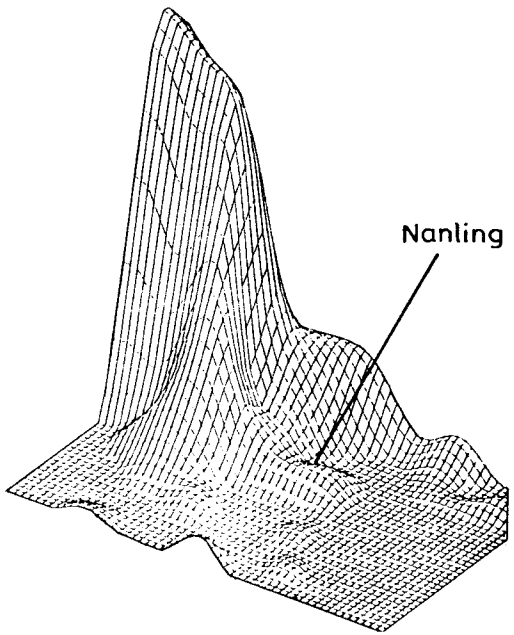

Figure 6 Topography (TG) of the JMA Global Spectral Model

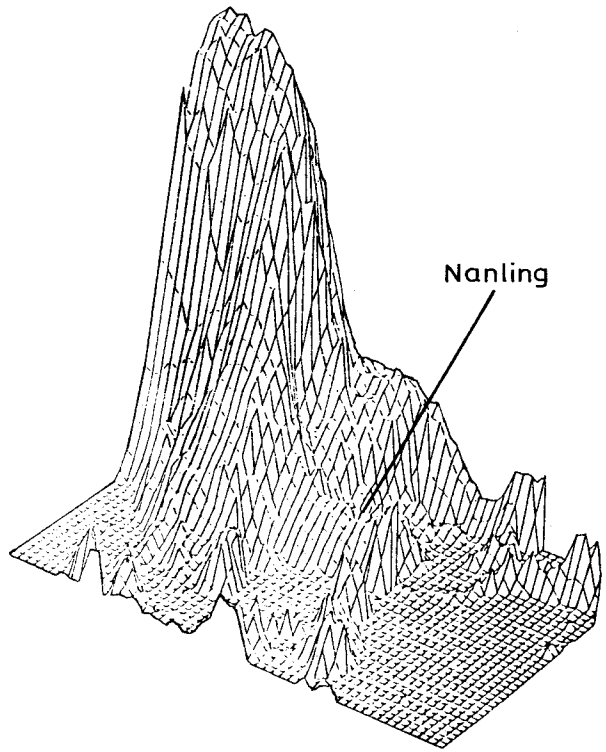

Figure 7 Envelope topography (TE) of the Royal Observatory limited area model

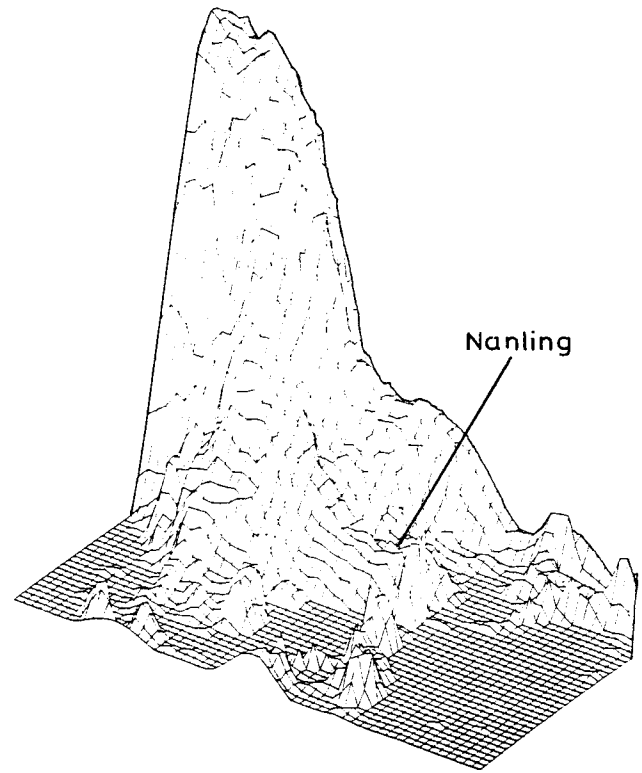

Figure 8 Combined topography (T)

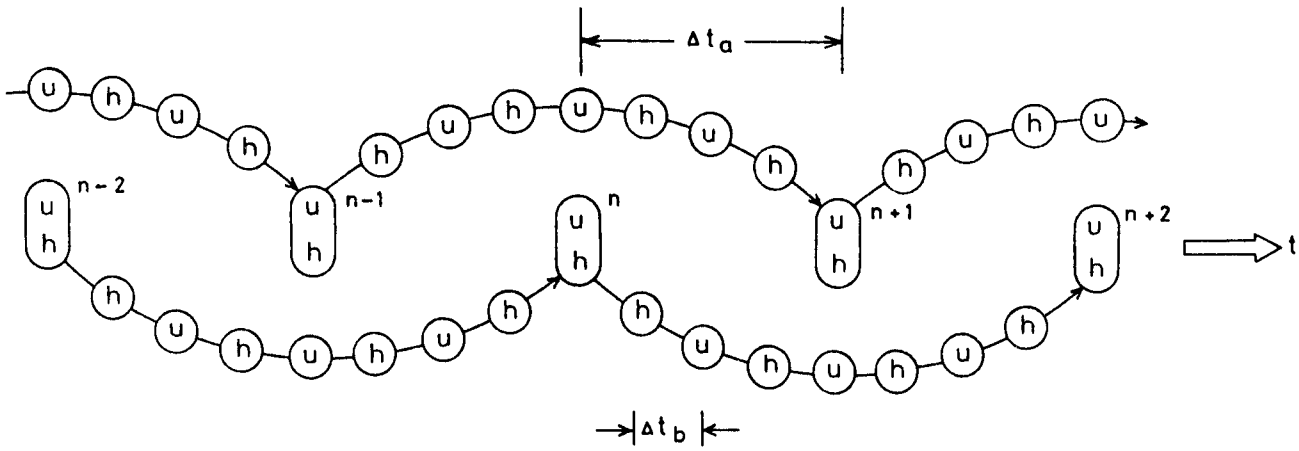

Figure 9 Flow of Tatsumi's economic explicit time integration scheme

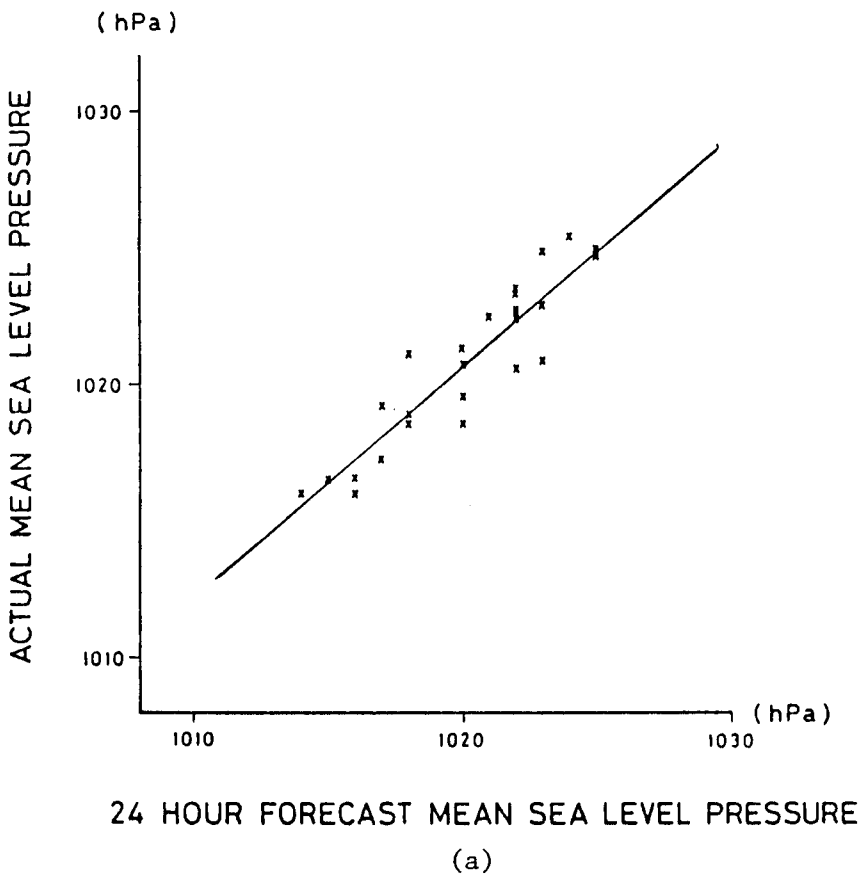

(a)

Figure 10 Accuracy of forecast mean sea level pressure

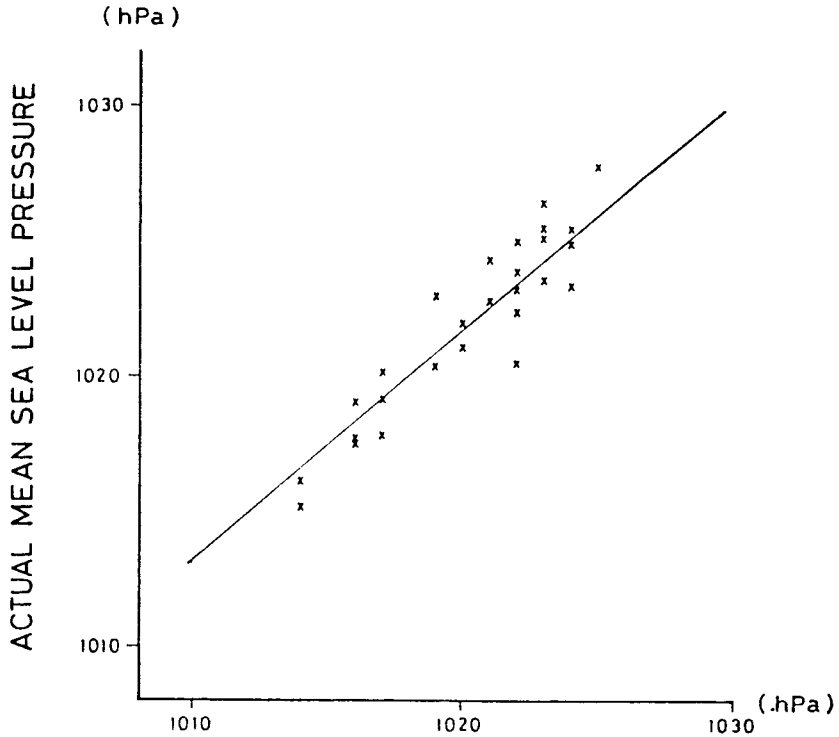

(b)

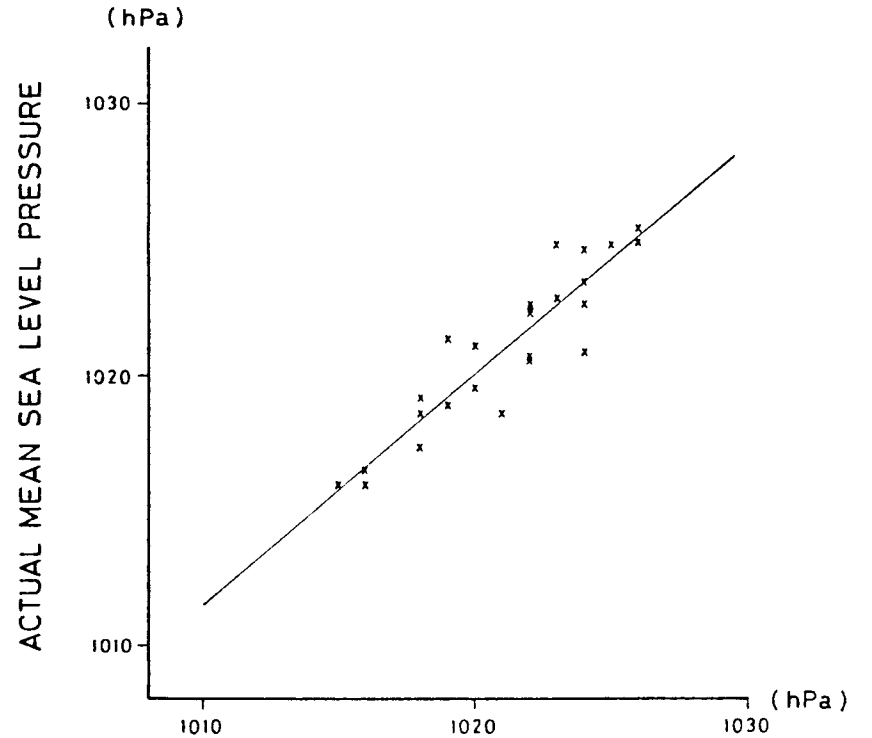

(c)

Figure 10 Accuracy of forecast mean sea level pressure

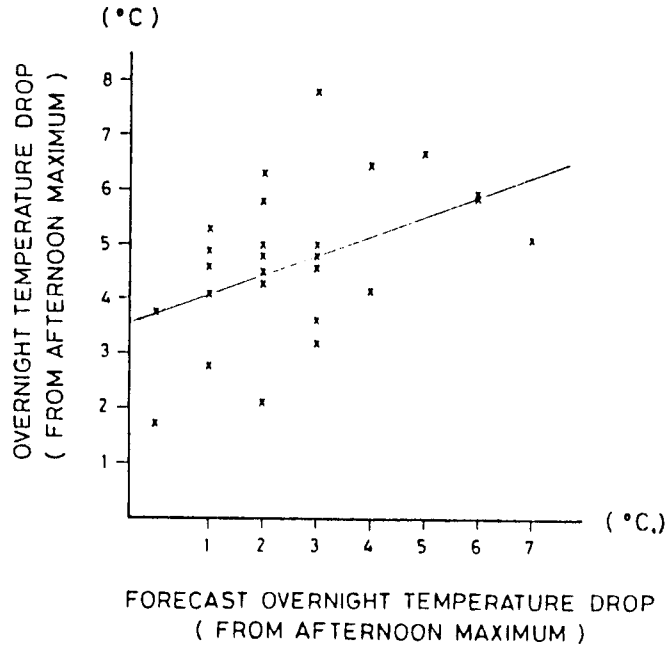

Figure 11 Accuracy of forecast overnight temperature drop from afternoon maximum

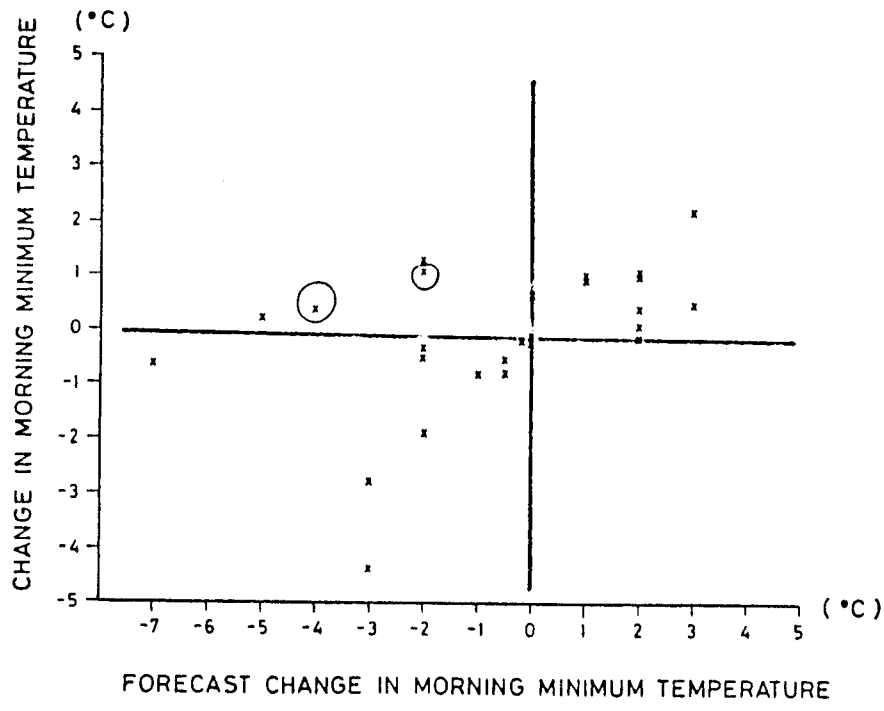

Figure 12 Accuracy of forecast change in morning minimum temperature

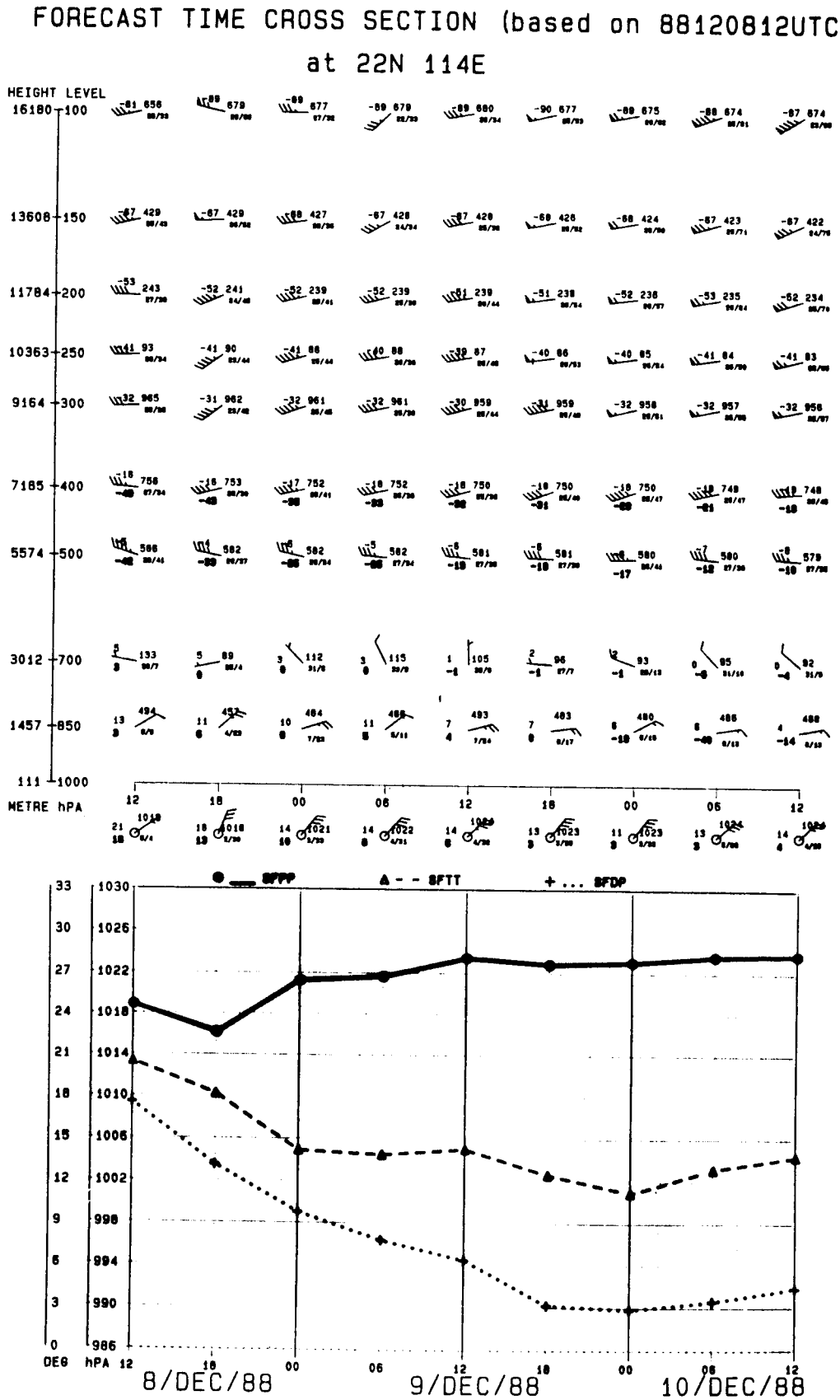

(a) forecast

Figure 13 Drying up on the 850/700 hPa levels

(b) actual

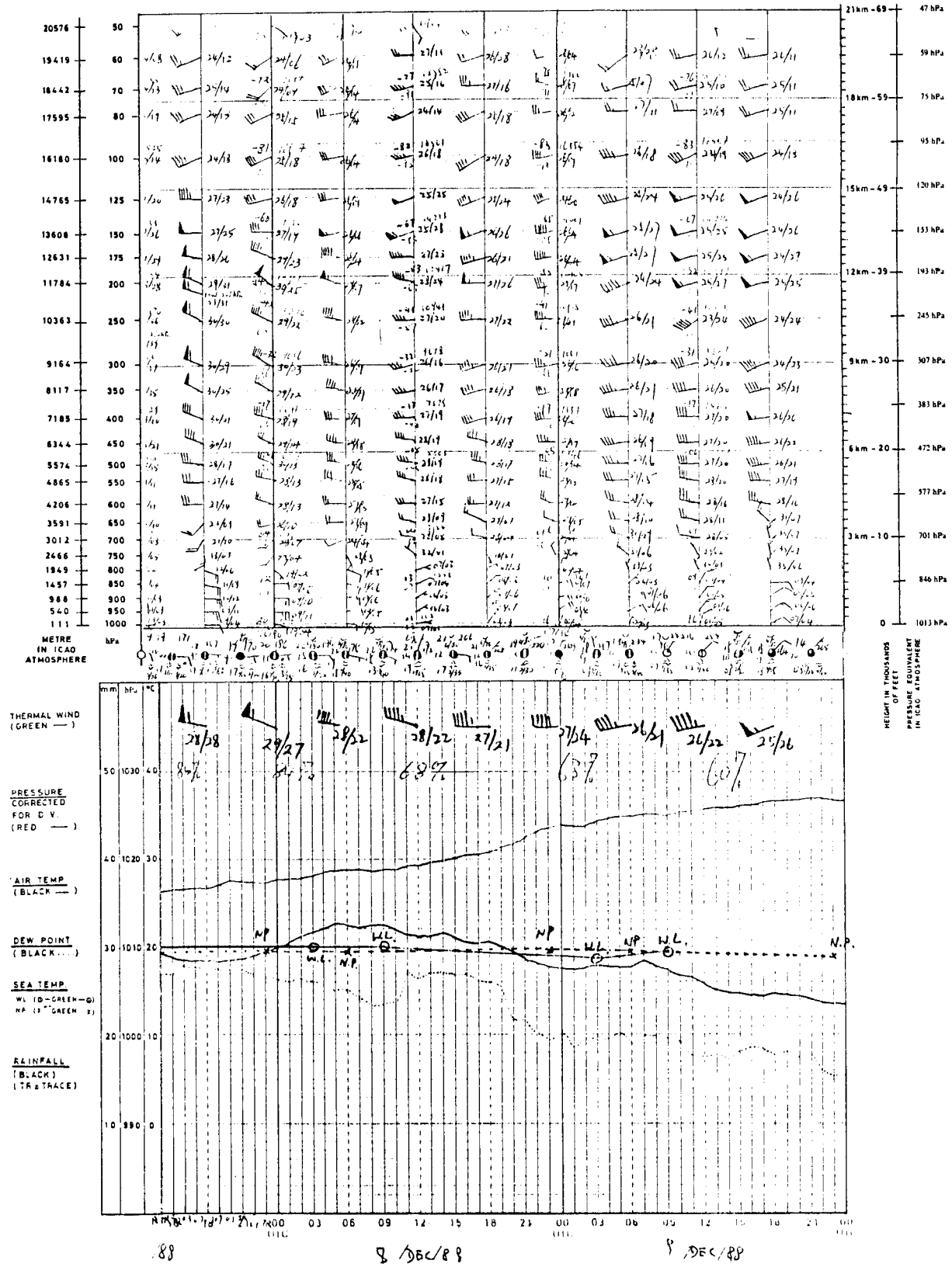

Figure 13 Drying up on the 850/700 hPa levels

(b) actual (con't)

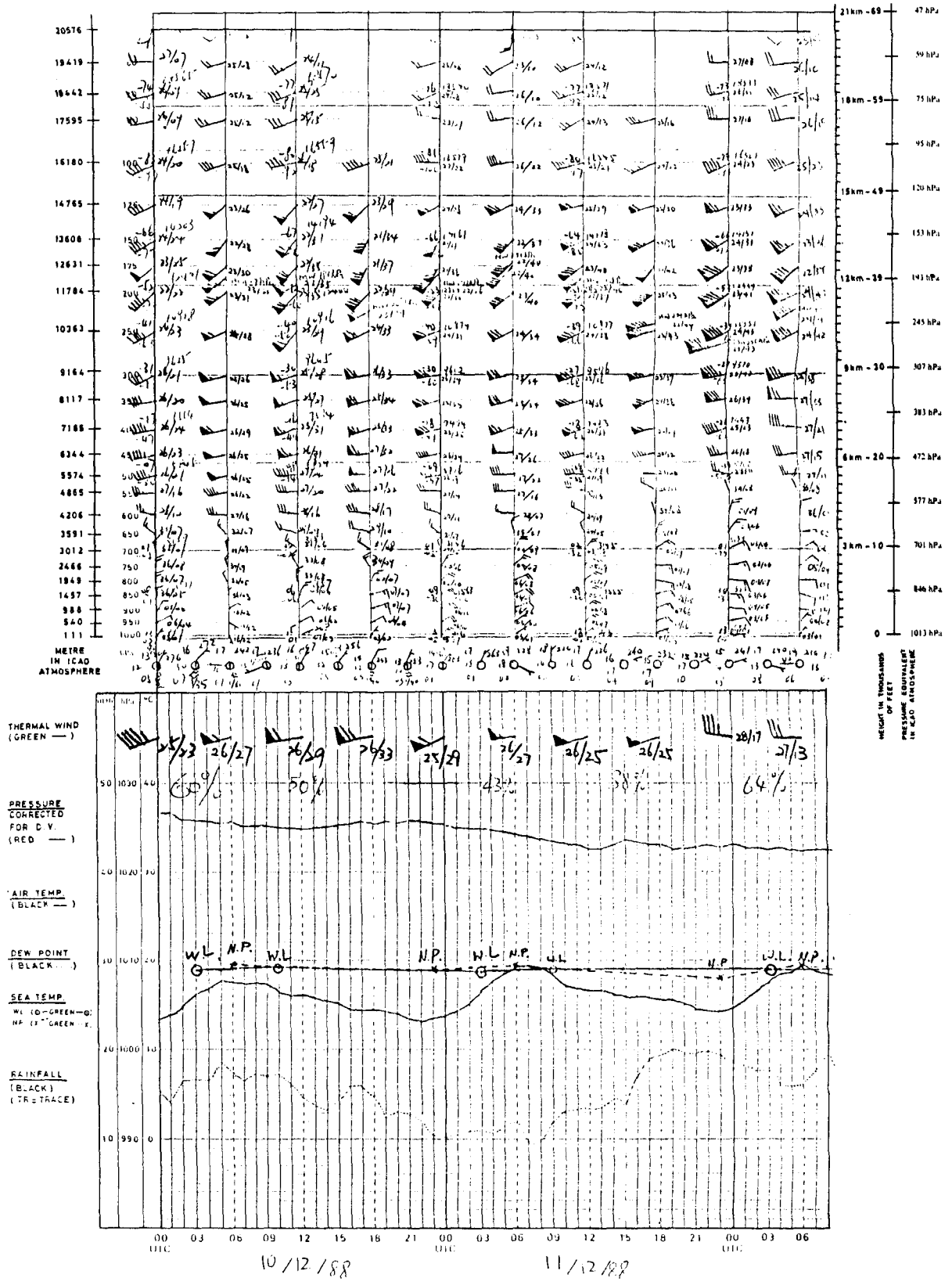

Figure 13 Drying up on the 850/700 hPa levels

levels	sigma	p(hPa)
1	0.995	10
2	0.978	20
3	0.950	30
4	0,910	40
5	0.861	50
6	0.800	60
7	0,728	70
8	0.644	80
9	0.550	90
10	0.444	100
11	0.328	110
12	0,200	120
13	0.067	120

Table 1 The sigma levels and the approximate thickness of each layer of the Royal Observatory limited area model